Some New Insights of Rock Failure under Dynamic Loading

J. Zhao and Q.B. Zhang

Department of Civil Engineering, Monash University, Clayton, VIC 3800, Australia
jian.zhao@monash.edu, qianbing.zhang@monash.edu

Abstract

Experimental investigations are conducted to study dynamic fracture behaviour of sedimentary, igneous and metamorphic rocks. The notched semi-circular bending method (NSCB) has been employed to determine fracture parameters using a split Hopkinson pressure bar (SHPB). The time to fracture, crack speed and velocity of the flying fragments are measured by strain gauge, crack propagation gauge and high-speed photography. Dynamic crack initiation toughness is determined from the dynamic stress intensity factor at the time to fracture, and dynamic crack growth toughness is derived by dynamic fracture energy at a specific crack speed. This study reveals clearly that (i) dynamic crack initiation and growth toughness increase with increasing loading rate and crack speed; (ii) kinetic energy of the flying fragments increases with increasing impact speed of the striker; and, (iii) dynamic fracture energy increases rapidly with increasing crack speed. A semi-empirical rate-dependent fracture model is proposed.

Keywords: Rock Dynamics,Dynamic Loading,Failure Mechanisms, Fracture Toughness, Energy

1. Introduction

Mechanical properties and fracture behaviour of rock materials change with the loading rate, and in particular the responses distinguishably change after the loading rate exceeds a critical value (Bazant et al. 1993; Zhang and Zhao 2014a; Zhao et al. 1999; Zhou et al. 2012). Understanding the effects of loading rate relies on accurate measurements of the macroscopic phenomena and interpretation of failure micromechanisms in producing the observed phenomena.

The International Society for Rock Mechanics (ISRM) has suggested four standardized methods: chevron bend (CB) and short rod (SR) methods, cracked chevron notched Brazilian disc (CCNBD) method, and NSCB method, for the determination of quasi-static fracture toughness. The fracture behaviour of rock materials under quasi-static loading is quite well understood (Atkinson 1987), however the studies under dynamic loading have been less investigated. Dynamic testing methods are basically extended from the corresponding quasi-static ones and categorized approximately into three main groups: Brazilian disc (BD) type, compact tension (CT) type and bending type methods (Zhang and Zhao 2014b). Due to the complication of data processing at intermediate loading rate, only a limited data are presented. At high loading rate, the SHPB has been used substantially, especially combining with high-speed optical measurement techniques. In this study, the NSCB method was employed to investigate dynamic fracture behaviour of rocks using a SHPB technique.

2. Experimental Procedures

2.1 Material Characterizations

We selected four types of rock material that were well studied in dynamic fracture tests for the comparison with previous studies, namely Sichuan calcareous sandstone, Fangshan gabbro, Ya'an coarse-grained (CG) marble and Fangshan fine-grained (FG) marble. Fig.1 showed the cross-polarized micrographs.

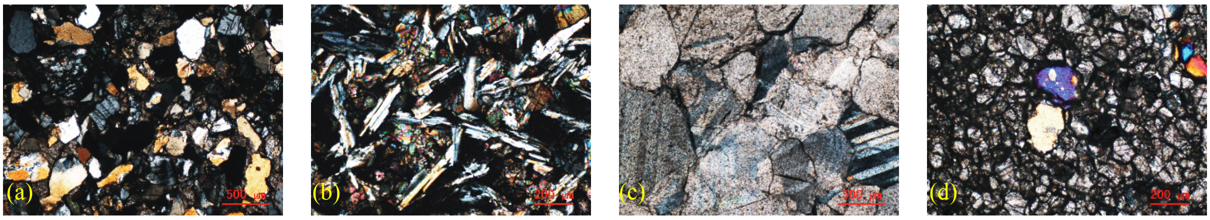

Fig. 1. Micrographs of(a) sandstone, (b) gabbro, (c) coarse-grained marble, (d) fine-grained marble

2.2 Testing Method and Measurement Techniques

All specimens of each rock type were drilled from one large block. Rock cores with a nominal diameter of 50 mm were drilled and sliced to obtain discs with an average thickness of 20 mm. The disc was split along the diameter into two semi-circular specimens and a 5 mm length edge notch was cut using a high-speed diamond impregnated circular blade. The notch tip was sharpened using a diamond wire saw to achieve a sharp crack tip.

Dynamic fracture tests were carried out using a SHPB system and the schematic representation of the experimental setup was shown in Fig. 2a. To systematically study the effect of loading rate, the striker was launched by a gas gun at speeds ranging from 2.0 to 5.0 m/s. Fig. 2b showed the photograph of loading configurations and a NSCB specimen with random speckle patterns on the surface that was applied to ensure good contrast of the images for calculating strain field using the digital image correlation (DIC) method. The high-speed camera was operated at the setting: 192×224 pixels for the size of 26×16 mm^2, and 125,000 frames per second. All the signals of strain gauges and the high-speed camera were synchronized with a threshold of the strain gauge signal on the incident bar. For further details the reader is referred to the previous publication (Zhang and Zhao 2013a).

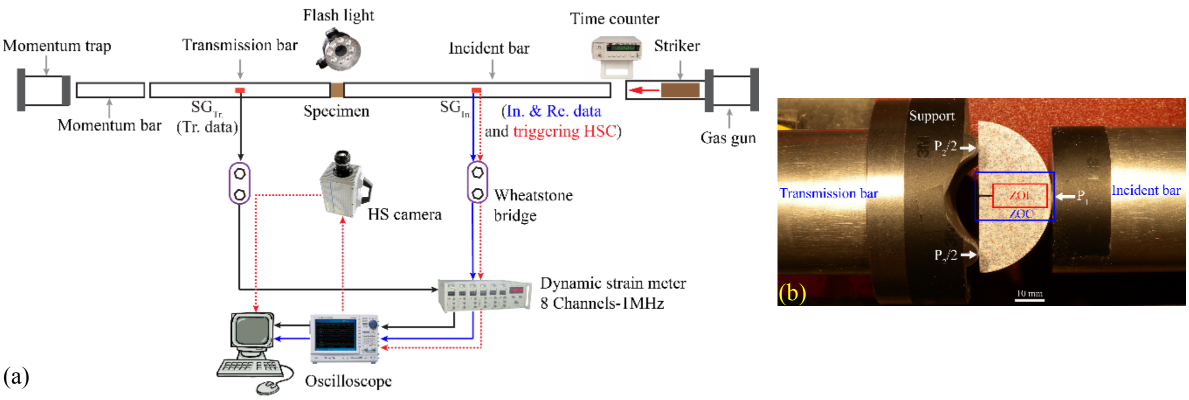

Fig. 2. Experimental techniques (modified after (Zhang and Zhao 2013a)), (a) schematic of the SHPB system (not to scale), (b) close-up view of the partial SHPB bars and a specimen with random speckle patterns (ZOI-Zone of interest, ZOC-Zone of camera)

3. Experimental Results

The dynamic crack initiation toughness K_{Id} is the critical dynamic SIF at the time to fracture t_{f}, and the dynamic crack growth toughness K_{ID} is the critical SIF at a specific crack speed v, which are given by the following equations (Ravi-Chandar 2004)

$$K_{\mathrm{Id}}(\dot{K}_{\mathrm{I}}^{\mathrm{dyn}}) = K_{\mathrm{I}}^{\mathrm{dyn}}(t_{\mathrm{f}}) \quad \text{at} \quad t = t_{\mathrm{f}} \tag{1}$$

$$K_{\mathrm{ID}}(v; \dot{K}_{\mathrm{I}}^{\mathrm{dyn}}) = K_{\mathrm{I}}^{\mathrm{dyn}}(t, v) \quad \text{for} \quad t > t_{\mathrm{f}} \tag{2}$$

where the dynamic loading rate is generally expressed as $\dot{K}_{\mathrm{I}}^{\mathrm{dyn}} = K_{\mathrm{Id}} / t_{\mathrm{f}}$.

3.1 Time to Fracture

The time to fracture is defined as the time interval from the beginning of the loading phase to the onset of rapid crack propagation. Once the dynamic SIF is determined by an applicable method, the time to fracture is the most important factor that influences the result.In this study, $t_f$was primarily measured by high-speed photographs and calibrated by strain gauges or crack propagation gauge. Fig. 3 shows typical dynamic fracturing processes in gabbroat the impact velocity of 3 m/s. There are some distinct characteristics during crack propagation: undulated path in sandstone; straight fracture path in gabbro; unnoticeable ductile fracturing in coarse-grained marble; individual white belt emerged prior to the initiation of the macroscopic observable crack in fine-grained marble; and some small particles were obviously seen in sandstone and CG marble after crack completely split into two fragments. Except the straight cracking, the others would to some extent limit the crack speed. Experimental results of t_f are presented with crack initiation toughness in next section.

3.2 Dynamic Crack Initiation Toughness

It has been generally accepted that the fracture toughness of rock materials increases with increasing loading rate, though the normalized fracture toughness (the ratio of dynamic fracture toughness to quasi-static fracture toughness, K_{Id}/K_{IC}) is quite different.

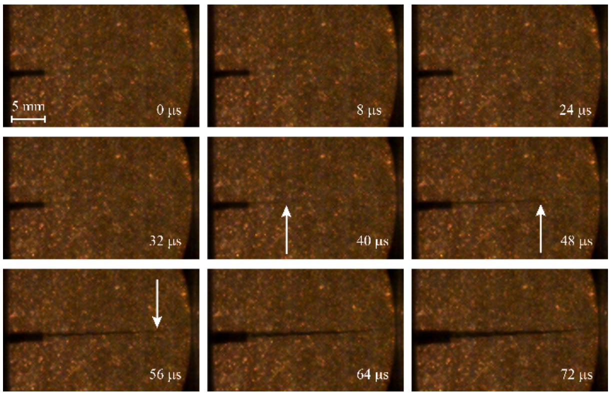

Fig. 3. High-speed photographs showing dynamic fracturing process of gabbro

It has been reported that the specimen is in a state of force equilibrium through the time to fracture t_f(Zhang and Zhao 2013b), and the dynamic crack initiation toughness $K_{Id}$is thus determined by Eq. 1 using the mean force applied on the specimen andt_f. The experimental dataof $K_{Id}/K_{IC}$and t_f are presented in Fig. 4, and the predictions by the analytical solutions with various critical distances (Liu et al. 1998)are also shown. It is observed from Fig. 4 that the degrees of normalized dynamic initiation toughness in gabbro and FG marble are apparently higher than that in sandstone and CG marble; the general trend of the experimental data corresponds well with the analytical prediction.

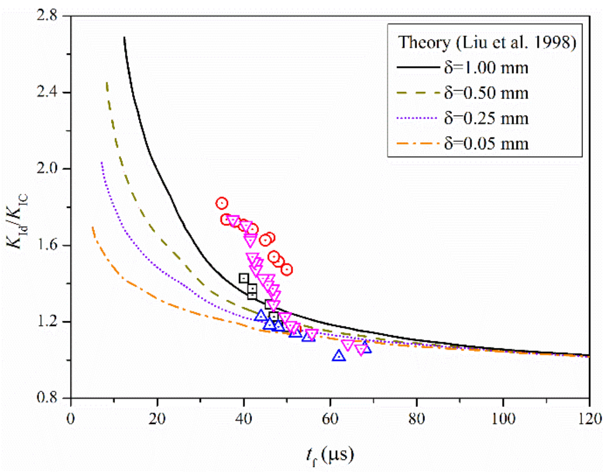

Fig. 4. Normalized dynamic crack initiation toughness $K_{Id}/K_{IC}$and time to fracture $t_f$of theoretical model (Liu et al. 1998) and experimental data

It should be noted that in Fig. 5 the K_{Id}/K_{IC} of rocks increased almost linearly with increasing normalized loading rates, but the effects of loading rate are dependent on rock microstructures.

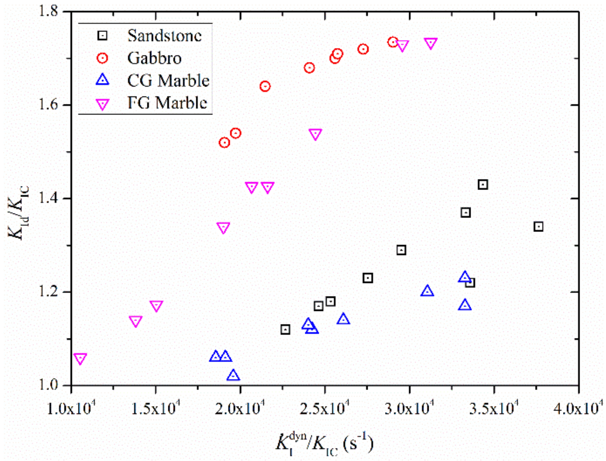

Fig. 5. Normalized dynamic crack initiation toughness as a function of normalized loading rate

3.3 Crack Speed

It has been found that once the limit of crack speed is reached, the phenomenon of crack branching takes place, i.e. the propagating crack forms additional multiple cracks at an angle to the original path (Ravi-Chandar 2004). The phenomena have been observed by many researchers in amorphous materials and the limiting crack speeds v_{lim} are in the range of $0.33C_R$ and $0.66C_R$(Ravi-Chandar 2004). Table 1presented asummary of crack speeds and the ratio v_{max}/C_R. The values of $v_{max}$are from $0.2C_R$to $0.71C_R$ at high loading rate. As reported in the previous publication (Zhang and Zhao 2013b), the crack speeds showed the same acceleration across the specimen with an initial increasing and then levelling off. The phenomena of macroscopic crack branching were not observed, perhaps due to the small size of the specimen and indirect tension of the testing method.

Table 1 Measured crack speeds in rock materials under dynamic loads

Rock type	v(m/s)	C_R(m/s)	v_{max}/C_R
Sandstone	300-650	1,800	0.36
Gabbro	430-1,120	3,200	0.35
CG Marble	280-480	1,450	0.33
FG Marble	320-1,000	2,640	0.38

3.4 Dynamic Fracture Energy

The determination of dynamic fracture energy is challenging at high loading rate due to the limitation of measurement techniques. In the SHPB test, the energies of incident wave $W_{In.}$, reflected wave $W_{Re.}$, and transmitted wave $W_{Tr.}$ are expressed, respectively (Zhang and Zhao 2014a)

$$W_{In.} = \frac{A_B C_B}{E_B}\int \varepsilon_{In.}(t)^2 \mathrm{d}t\,, \qquad W_{Re.} = \frac{A_B C_B}{E_B}\int \varepsilon_{Re.}(t)^2 \mathrm{d}t\,, \qquad W_{Tr.} = \frac{A_B C_B}{E_B}\int \varepsilon_{Tr.}(t)^2 \mathrm{d}t \quad (3)$$

where A_B is the cross-sectional area, C_B is the longitudinal wave speed, and E_B is the Young's modulus of the bars, andε is the strain measured by strain gauges on the bars (The subscripts In., Re. and Tr. correspond to the incident, reflected and transmitted pulse, respectively.).

The following factors should be carefully checked: the forces on both sides of the specimen are non-equilibrium during the period; the effect of multiple pulse wave should be well eliminated; and the friction between the specimen and the bars. In this study, the single pulse wave is achieved by means of a longer length of the incident bar and a momentum trap for quasi-brittle materials. There are three-point contacts in the NSCB method to transfer dynamic loads: one contact is between the incident bar and the top point of the specimen, and the other two contacts formed by two supporting pins and the specimen, as shown in Fig. 2b. During the test, the notch of the specimen opens up and meantime results in frictional force by the pins to resist the specimen separation. Lubricants were used on the bar/specimen interfaces to reduce the friction effect. The friction between the bars and the specimen can thus be ignored, and the energy W_{S} absorbed by the specimen is given

$$W_{\mathrm{S}} = W_{\mathrm{In.}} - W_{\mathrm{Re.}} - W_{\mathrm{Tr.}} \tag{4}$$

Continued to Fig. 3c, Fig. 6a shows high-speed photographs until the NSCB specimen completely splits into two almost equal fragments. Each flying fragment has a combined rotational and translational motion, and the angular velocity $\omega$and translational velocity v_{T} can be estimated from its local coordinates at each time step, as defined schematically in Fig. 6b. At the first stage, ωincreases with increasing time, while v_{T} shows a decreasing trend, as shown in Fig. 6c, which indicates obviously that the increase of the v_{T} are on the expense of the reduction of v_{T}. Then both velocities become constant and there is no change in the total kinetic energy. The total kinetic energy T, translational kinetic energy $T_{\mathrm{Tra.}}$, and rotational kinetic energy $T_{\mathrm{Rot.}}$ can thus be correlated by

$$T = 2(T_{\mathrm{Tra.}} + T_{\mathrm{Rot.}}) = m v_{\mathrm{T}}^2 + I\omega^2 \tag{5}$$

where $m$is the mass of one fragment, and $I = \frac{R^2}{36\pi^2}(9\pi^2 + 18\pi - 128)m$ is the moment of inertia around the axis of rotation.

The absorbed energy W_{S}can be partitioned primarily into the kinetic energy of the flying Fig. 6d shows the results of the total kinetic energy $T$and the absorbed energy W_{S}under three striking impact speeds $V_{\mathrm{Str.}}$. The absorbed energy $W_{\mathrm{S}}$is primarily partitioned into three parts: the total kinetic energy $T$of the flying fragments; the dissipated energy Ω that is associated with fracture surface and micro-cracks; and other energy, such as thermal energy. The loading rate in the present study is not very high, and thus other energy is assumed to be very small and negligible for the results. Therefore, the dissipated energy is obtained by Ω=W_{S}-T(see the top left inset in Fig. 6d), and the dynamic fracture energy (dissipated per unit area ∂A created)is written as $G_{\mathrm{dC}}=\partial\Omega/\partial A$. To simplify, the experimental measurable quantity A_{S} (i.e. the actual area of the fractured surface), and the calculated Ω are used to estimate the average fracture energy. The measurement of surface topography is conducted by a 3D laser profilometry and the approximate area ofA_{S} is estimated using the triangular prism surface area method. As shown in Fig. 6d, the values of the absorbed energy W_{S} are apparently higher than the total kinetic energy T with increase of the impact speed $V_{\mathrm{Str.}}$. With the assumption of the conservation of energy, the dissipated energy for creating fracture surface and micro-cracks is increased with the range of impact speeds. A fundamental aim of the study of a stationary crack under dynamic loading is examine the energy balance equation and the crack-tip equation of motion (Ravi-Chandar 2004). Fig. 6e shows the dynamic fracture energy approaches to a low level when the crack speed$v$is small and increases rapidly with the increase of v, which reveals that rock materials have the property of the crack speed-toughening. A phenomenological rate-dependent fracture energy that is a function of crack speed $G_{\mathrm{dC}}(v)$is broadly accepted Dally et al. (1985). For a mode I crack, when the crack speed $v$approaches to Rayleigh wave speed C_{R}, the dynamic fracture energy becomes very large. The observed limiting speeds v_{lim} are significantly smaller than C_{R}in nominally brittle materials (Ravi-Chandar 2004). As discussed previously, there is still lacking of limiting speeds v_{lim} for rock-like materials. Therefore, a semi-empirical rate-dependent model is proposed for the simulation of crack propagation in rock materials using the ratio of a theoretical characteristic velocityv_0 (assuming as a material constant) toC_{R}. The relationship between $G_{\mathrm{dC}}(v)$and $v$plotted in Fig. 6eis fitted by a two-parameters expression as follow

$$G_{\mathrm{dC}}(v) = G_{\mathrm{C}} e^{bv} \tag{6}$$

Where G_{C} is quasi-static fracture energy, and$b$is a material constant, b=0.01v_0/C_{R}. The values of b for sandstone, gabbro, coarse-grained marble and fine-grained marble are 0.0048, 0.003, 0.0038 and

0.004, respectively. Thus, the corresponding theoretical characteristic velocities v_0 are 864, 960, 551, and 1,056 m/s, which are nearly as the same as the measured maximum crack speeds v_{max}.

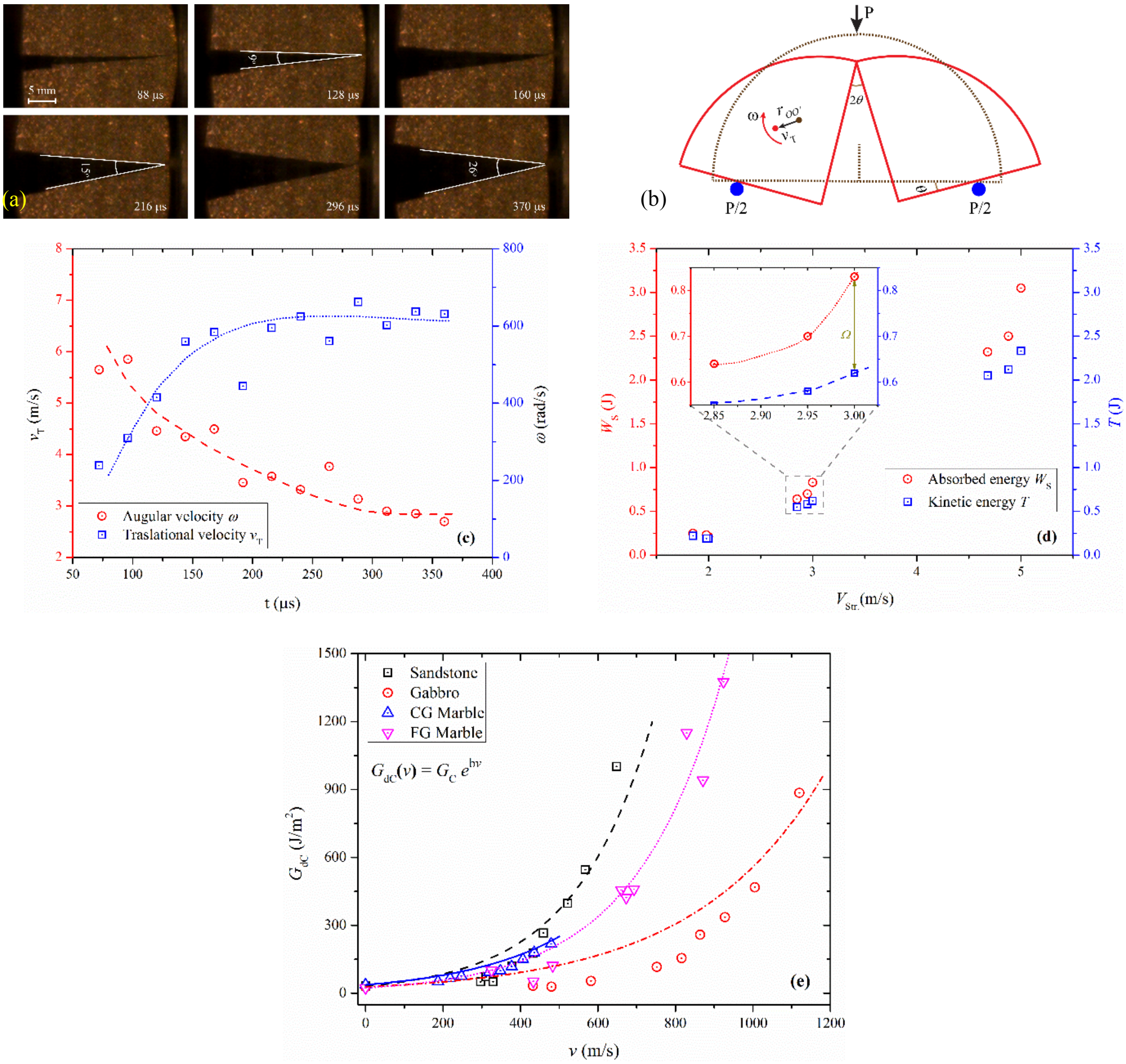

Fig. 6(a). High-speed photographs of the movement of the flying fragments after impact (continuing on Fig. 3), (b) schematic of the fracturing specimen (*O*is the center of mass, $r_{OO'}$is the distance of translational movement), (c) translational and angular velocity of the flying fragments, (d) comparison of kinetic energy of flying fragments with absorbed energy of gabbro, (e) dynamic fracture energy as a function of crack speed

3.5 Dynamic Crack Growth Toughness

Pioneering research on dynamic crack growth toughness K_{ID} was performed on Solnhofen limestone using a projectile impact technique and an on-specimen strain gauge (Bertram and Kalthoff 2003). We attempted to use the method of strain gauge to determine the dynamic SIF, but the results were hardly repeatable, perhaps due to the heterogeneity of rocks. In the SHPB test, the forces at two sides of the specimen are non-equilibrium after the time to fracture (Zhang and Zhao 2013a), and the dynamic SIF becomes a function of crack speed. Due to the limitation of the speed and resolution of high-speed camera, it is still challenging to measure the dynamic displacement fields in quasi-brittle opaque materials. Thus, indirect method were applied to estimate the K_{ID}, for example, on the basis of well-known Irwin's correlation $K_{ID} = \sqrt{G_{dC}E/(1-\mathbf{v}^2)}$. It should be noted that, however, when a crack propagated dynamically, the dynamic energy release rate $G_d(t, v)$is related to the dynamic SIF $K_I^{dyn}(t, v)$(Ravi-Chandar 2004)

$$G_{\mathrm{d}}(t,v)=A_{\mathrm{I}}(v)\frac{1-\mathbf{v}^2}{E}[K_{\mathrm{I}}^{\mathrm{dyn}}(t,v)]^2 \tag{7}$$

Thus, the dynamic crack growth toughness K_{ID} at a specific crack speed is rated to the critical G_{dC} via

$$K_{\mathrm{ID}}=\sqrt{\frac{1}{A_{\mathrm{I}}(v)}\frac{G_{\mathrm{dC}}E}{1-\mathbf{v}^2}} \tag{8}$$

where $A_{\mathrm{I}}(v)=\dfrac{v^2\alpha_{\mathrm{d}}}{(1-\mathbf{v})C_{\mathrm{S}}^2R(v)}$, $\alpha_{\mathrm{d}}=\sqrt{1-\dfrac{v^2}{C_{\mathrm{L}}^2}}$, $\alpha_{\mathrm{s}}=\sqrt{1-\dfrac{v^2}{C_{\mathrm{S}}^2}}$, $R(v)=4\alpha_{\mathrm{d}}\alpha_{\mathrm{s}}-(1+\alpha_{\mathrm{s}}^2)^2$.

The normalized dynamic crack growth toughness $K_{\mathrm{ID}}/K_{\mathrm{IC}}$ increases with the normalized crack speed v/C_{R}(see Fig. 7).Experimental results are summarized in Table 7, including loading rate $\dot{K}_{\mathrm{I}}^{\mathrm{dyn}}$, the time to fracture t_{f}, dynamic crack initiation toughness K_{Id}, crack speed$v$, kinetic energy of fragments T, dissipated energy Ω, dynamic fracture energyG_{dC}, and calculated dynamic crack propagation toughnessK_{ID}.

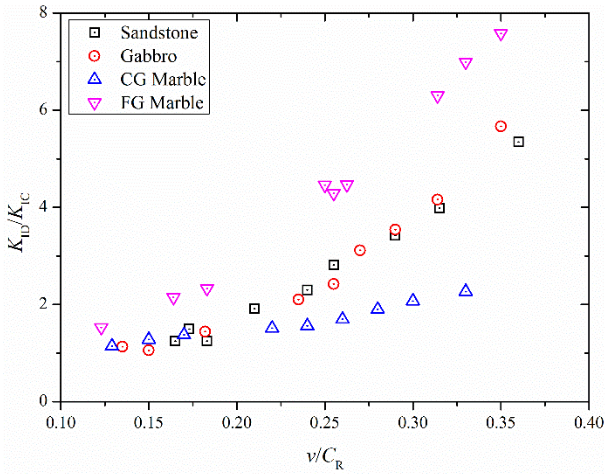

Fig. 7. Normalized dynamic crack growth toughness as a function of normalized crack speed

4. Conclusions

Notched semi-circular bending tests were performed to study quasi-static and dynamic fracture behaviour of four well-studied rock types. On-specimen strain gauges and high-speed photography were used to determine dynamic fracture parameters at the macroscopic scale. The fracture surfaces were qualitatively and quantitatively investigated by conducting fractographic examination and roughness measurements. The main conclusions of this study are as follows:

(1) The dynamic crack initiation toughness was obtained from the quasi-static analysis that was evidenced by the force equilibrium until the time to fracture. The crack speed and velocity of flying fragments were quantitatively determined from high-speed photographs. The dynamic fracture energy was estimated from the velocity of flying fragments, the absorbed energy and fracture surface area of the specimen, which increased rapidly with the increase of crack speed. The dynamic crack growth toughness was then derived from well-known Irwin's correlation at a specific crack speed.

(2) The dynamic crack initiation and growth toughness of four rock types were dependent on the loading rate, and the rate-sensitivity of growth toughness was more evident than that of the former. The degrees of normalized crack initiation toughness in gabbro and fine-grained marble were apparently higher than those in sandstone and coarse-grained marble, which were mainly governed by the time of stress wave required to travel through the specimen. The higher growth toughness was associated with a greater degree of transgranular microcracks.

Acknowledgements

This work was supported by the Swiss National Science Foundation (No. 200020_129757) and 2015 Engineering Seed Funding Scheme of Monash University.

References

Atkinson BK (ed) (1987) Fracture mechanics of rock. Academic Press, London

Bazant ZP, Bai SP, Gettu R (1993) Fracture of rock: Effect of loading rate. *EngFractMech* 45 (3):393-398. doi:10.1016/0013-7944(93)90024-m

Bertram A, Kalthoff JF (2003) Crack propagation toughness of rock for the range of low to very high crack speeds. *Key Eng Mater* 251-252:423-430. doi:10.4028/www.scientific.net/KEM.251-252.423

Dally JW, Fourney WL, Irwin GR (1985) On the uniqueness of the stress intensity factor-crack velocity relationship. *Int J Fract* 27 (3):159-168. doi:10.1007/bf00017965

Liu C, Knauss WG, Rosakis AJ (1998) Loading rates and the dynamic initiation toughness in brittle solids. *Int J Fract* 90 (1):103-118. doi:10.1023/a:1007447603177

Ravi-Chandar K (2004) Dynamic fracture. Elsevier Science,

Zhang QB, Zhao J (2013a) Effect of loading rate on fracture toughness and failure micromechanisms in marble. *EngFractMech* 102:288-309. doi:10.1016/j.engfracmech.2013.02.009

Zhang QB, Zhao J (2013b) Determination of mechanical properties and full-field strain measurements of rock material under dynamic loads. *Int J Rock Mech Min* 60:423-439. doi:10.1016/j.ijrmms.2013.01.005

Zhang QB, Zhao J (2014a) A review of dynamic experimental techniques and mechanical behaviour of rock materials. *Rock Mech Rock Eng* 47(4):1411-1478. doi:10.1007/s00603-013-0463-y

Zhang QB, Zhao J (2014b) Quasi-static and Dynamic Fracture Behaviour of Rock Materials: Phenomena and Mechanisms. *Int J Fract*, 2014, 189(1): 1-32.doi: 10.1007/s10704-014-9959-z

Zhao J, Zhou YX, Hefny AM, Cai JG, Chen SG, Li HB, Liu JF, Jain M, Foo ST, Seah CC (1999) Rock dynamics research related to cavern development for ammunition storage. TunnUndergrSp Tech 14 (4):513-526. doi:10.1016/s0886-7798(00)00013-4

Zhou YX, Xia K, Li XB, Li HB, Ma GW, Zhao J, Zhou ZL, Dai F (2012) Suggested methods for determining the dynamic strength parameters and mode-I fracture toughness of rock materials. Int J Rock Mech Min 49:105-112. doi:10.1016/j.ijrmms.2011.10.004